Constraining primordial non-Gaussianity via a multitracer technique with surveys by Euclid and the Square Kilometre Array

Daisuke Yamauchi,[1,*] Keitaro Takahashi,[2] and Masamune Oguri[1,3,4]

[1]*Research Center for the Early Universe, Graduate School of Science, The University of Tokyo, Bunkyo-ku, Tokyo 113-0033, Japan*

[2]*Faculty of Science, Kumamoto University, 2-39-1 Kurokami, Kumamoto 860-8555, Japan*

[3]*Department of Physics, The University of Tokyo, Bunkyo-ku, Tokyo 113-0033, Japan*

[4]*Kavli Institute for the Physics and Mathematics of the Universe, The University of Tokyo, Kashiwa, Chiba, 277-8568, Japan*

(Received 29 July 2014; published 20 October 2014)

We forecast future constraints on local-type primordial non-Gaussianity parameter $f_{\rm NL}$ with a photometric galaxy survey by Euclid, a continuum galaxy survey by Square Kilometre Array (SKA), and their combination. We derive a general expression for the covariance matrix of the power spectrum estimates of multiple tracers to show how the so-called multitracer technique improves constraints on $f_{\rm NL}$. In particular we clarify the role of the overlap fraction of multiple tracers and the division method of the tracers. Our Fisher matrix analysis indicates that stringent constraints of $\sigma(f_{\rm NL}) \lesssim 1$ can be obtained even with a single survey, assuming five mass bins. When Euclid and SKA phase 1 (2) are combined, constraints on $f_{\rm NL}$ are improved to $\sigma(f_{\rm NL}) = 0.61(0.50)$.

DOI: 10.1103/PhysRevD.90.083520 PACS numbers: 98.80.Es, 95.80.+p, 98.65.Dx

I. INTRODUCTION

Primordial non-Gaussianity of density fluctuations is key to understanding the physics of the early Universe. Among several types of primordial non-Gaussianity, the local-type one, $f_{\rm NL}$, has been studied widely, partly because even the simplest inflationary models predict small but nonvanishing values of $f_{\rm NL}$ of $\mathcal{O}(0.01)$. Here we quantify non-Gaussianity of the local form as

$$\Phi = \phi + f_{\rm NL}(\phi - \langle\phi^2\rangle), \tag{1}$$

where Φ and ϕ denote the Bardeen potential and an auxiliary random-Gaussian field.

Primordial non-Gaussianity has primarily been constrained from the bispectrum in cosmic microwave background (CMB) temperature fluctuations. Recently, Planck [1] obtained a tight constraint of $f_{\rm NL} = 2.7 \pm 5.8$ at 1σ statistical significance. A complementary way to access non-Gaussianity is to measure its impact on a large scale structure. Luminous sources such as galaxies must be most obvious tracers of the underlying dark matter distributions with a bias. Primordial non-Gaussianity induces the scale-dependent bias [2,3] such that the effect dominates at very large scales. Hence, based on a reasonable assumption that the galaxy bias is linear and deterministic on large scales, it has been shown that the galaxy survey can effectively constrain $f_{\rm NL}$ to the level comparable to CMB temperature anisotropies [4,5]. While clustering analyses at large scales are limited due to cosmic variance, Seljak [6] proposed a novel method to reduce the cosmic variance using multiple tracers with different biases, the so-called multitracer technique. This method allows us to measure the scale-dependent bias accurately even at large scales, leading to strong constraints on $f_{\rm NL}$.

Future wide and deep surveys with Euclid[1] in optical and infrared bands and Square Kilometre Array (SKA)[2] in radio wavelengths will provide an unprecedented number of galaxies to measure the power spectra. The radio continuum survey conducted with SKA covers $30,000$ deg^2 out to high redshifts, though the redshift information is not available. The authors in [7] found that even without the redshift information the multitracer technique improves constraints as $\sigma(f_{\rm NL}) = \mathcal{O}(1)$, while weaker constraints of $\sigma(f_{\rm NL}) = \mathcal{O}(10)$ without the multitracer technique. While the number of galaxies and covered area are smaller for the Euclid photometric survey ($15,000$ deg^2), it provides redshift information via photometric redshifts. Redshift information is expected to be highly advantageous for constraining $f_{\rm NL}$ because the bias evolves strongly with redshift. As we show below, each of these two surveys provides constraints of $\sigma(f_{\rm NL}) = \mathcal{O}(1)$, and constraints improve to $\sigma(f_{\rm NL}) = \mathcal{O}(0.1)$ with their combination. To calculate expected constraints, in this paper, we employ the Fisher matrix formalism including the redshift binning as well as the mass binning, taking the overlap of the two survey regions into account.

*yamauchi"at"resceu.s.u-tokyo.ac.jp

[1]See http://www.euclid-ec.org.

[2]See http://www.skatelescope.org.

II. PRIMORDIAL NON-GAUSSIANITY IN THE LARGE SCALE STRUCTURE CLUSTERING

First, we consider the non-Gaussian correction of the halo bias given by [3]

$$\Delta b = \frac{2 f_{\rm NL}\delta_{\rm c}}{\mathcal{M} D_+}(b_{\rm L}-1) - \frac{1}{\delta_{\rm c}}\frac{\rm d}{{\rm d}\ln\nu}\left(\frac{{\rm d}n/{\rm d}M}{{\rm d}n_{\rm G}/{\rm d}M}\right), \quad (2)$$

where $\nu = \delta_c/\sigma$, $\delta_{\rm c} \approx 1.68$ is the critical linear density for spherical collapse and $\sigma(M,z) = \sigma_R(z)$ is the variance of the linear density field smoothed on the scale $R(M) = (3M/4\pi\rho_{\rm b,0})^{1/3}$ with $\rho_{\rm b,0}$ being the background density today. $D_+(z)$ is the growth factor, $\mathcal{M}(k) = 2k^2T(k)/3\Omega_{\rm m,0}H_0^2$, where $T(k)$ is the matter transfer function normalized to unity at large scales [8]. We employ a fit to simulation for the Gaussian mass function ${\rm d}n_{\rm G}/{\rm d}M$ and the linear bias factor $b_{\rm L}$ given in [9]. We adopt a non-Gaussian correction of the mass function developed in [10], where we need the skewness of the density field that is proportional to $f_{\rm NL}$ [3,11,12]. In this paper, for σS_3, we adopt a fitting formula from [11].

Constraints on $f_{\rm NL}$ come from the redshift and mass dependences of the bias. Thus, in order to take advantage of the multitracer technique, we need a rough estimate of the halo mass of each galaxy. In the Euclid survey, assuming an accurate photometric redshift estimate of each galaxy, we can use various galaxy properties such as luminosity, color, and stellar mass to infer the halo mass. See e.g. [13,14] for details. On the other hand, it is more challenging to estimate the halo mass of galaxies from radio surveys. In this paper, following [7], we assume that halo mass can be estimated from the galaxy type.

Estimates of the halo mass for individual galaxies involve large uncertainties. We take account of the uncertainties in halo mass estimation following [15]. Given the estimated mass $M_{\rm est}$, the probability that the true mass is M is assumed to be given by log-normal distribution with the variance $\sigma^2_{\ln M}$ and the bias $\ln M_{\rm bias}$,

$$x(M_{\rm est};M) = \frac{\ln M_{\rm est} - \ln M - \ln M_{\rm bias}}{\sqrt{2}\sigma_{\ln M}}. \quad (3)$$

Furthermore, it is expected that these parameters depend on both halo mass and redshift. We assume the following functional form [16,17]:

$$\ln M_{\rm bias}(M,z) = \ln M_{\rm b,0} + \sum_{i=1}^{3} q_{{\rm b},i}\left[\ln\left(\frac{M}{M_{\rm piv}}\right)\right]^i + \sum_{i=1}^{3} s_{{\rm b},i} z^i, \quad (4)$$

$$\sigma_{\ln M}(M,z) = \sigma_{\ln M,0} + \sum_{i=1}^{3} q_{\sigma_{\ln M},i}\left[\ln\left(\frac{M}{M_{\rm piv}}\right)\right]^i + \sum_{i=1}^{3} s_{\sigma_{\ln M},i} z^i, \quad (5)$$

with $M_{\rm piv} = 10^{12}h^{-1}M_\odot$. Here we included a large number of parameters that model the uncertainty of the halo mass estimate, which are fully marginalized over when deriving constraints on $f_{\rm NL}$.

To apply the multitracer technique, we split galaxy samples into N_M mass-divided subsamples for each redshift bin. The average density of galaxies in the ith redshift bin $z_i < z < z_{i+1}$ and the bth mass bin $M_{(b)} < M_{\rm est} < M_{(b+1)}$ is given by

$$\bar{N}_{i(b)} = \int_0^\infty {\rm d}z \frac{{\rm d}^2V}{{\rm d}z{\rm d}\Omega}\int_0^\infty {\rm d}M \frac{{\rm d}n}{{\rm d}M} S_{i(b)}. \quad (6)$$

Here ${\rm d}^2V/{\rm d}z{\rm d}\Omega = \chi^2/H$ denotes the comoving volume element per unit redshift per unit steradian, and we have introduced $S_{i(b)}(M,z)$ to represent the selection function:

$$S_{i(b)}(M,z) = \Gamma_{(b)}\Theta(z-z_i)\Theta(z_{i+1}-z) \times \frac{1}{2}[{\rm erfc}(x(M_{(b)};M)) - {\rm erfc}(x(M_{(b+1)};M))], \quad (7)$$

where we have introduced the gray-body factor $\Gamma_{(b)}$ to denote the fraction of observed halos for each mass bin, since we may not be able to observe all galaxies associated with the underlying dark matter halos. With these variables, the Limber-approximated angular power spectrum between b- and $b\prime$th mass bins in the ith redshift bin is expressed by [16]

$$C_{i(bb\prime)}(\ell) = \int_0^\infty {\rm d}z W_{i(b)} W_{i(b\prime)} \frac{H}{\chi^2} P_\delta\left(\frac{\ell+1/2}{\chi}, z\right), \quad (8)$$

where $P_\delta(k,z)$ is the underlying dark matter power spectrum and $W_{i(b)}$ is the weight function defined as

$$W_{i(b)} = \frac{1}{\bar{N}_{i(b)}}\frac{{\rm d}^2V}{{\rm d}z{\rm d}\Omega}\int_0^\infty {\rm d}M \frac{{\rm d}n}{{\rm d}M} S_{i(b)} b_h\left(M, z, \frac{\ell+1/2}{\chi}\right). \quad (9)$$

III. FISHER MATRIX FORMALISM

We adopt the Fisher analysis to estimate expected errors of model parameters for a given survey. The Fisher matrix is defined by

$$F_{\alpha\beta} = \sum_{\ell=\ell_{\rm min}}^{\ell_{\rm max}} \sum_{I,J} \frac{\partial C_I(\ell)}{\partial\theta^\alpha} [{\rm Cov}(\boldsymbol{C}(\ell), \boldsymbol{C}(\ell))]^{-1}_{IJ} \frac{\partial C_J(\ell)}{\partial\theta^\beta}, \tag{10}$$

where the indices I and J run over the redshift and mass bin, $(i,\ b,\ b\prime)$, and θ^α are model parameters. Here, we consider 29 parameters in the Fisher matrix analysis: the primordial non-Gaussianity parameter $f_{\rm NL}$, 14 parameters for systematic errors in the halo mass estimate for each of Euclid and SKA [see Eqs. (4) and (5)]. We choose $\sigma_{\ln M,0} = 0.3$ and zero for the other parameters as fiducial values. On the other hand, we fix standard cosmological parameters to those of the standard ΛCDM model: $\Omega_{\rm m,0} = 0.266$, $\Omega_{\rm b,0} = 0.04479$, $\Omega_\Lambda = 0.734$, $w = -1$, $h = 0.710$, $n_{\rm s} = 0.963$, $k_0 = 0.05\ {\rm Mpc}^{-1}$ and $\sigma_8 = 0.801$. The marginalized error on each parameter is given by $\sigma(\alpha) = \sqrt{(\boldsymbol{F}^{-1})_{\alpha\alpha}}$.

Now we derive the covariance matrix generalized to multiple tracers which are observed in different sky areas with some overlap. We introduce the observed density contrast as

$$\delta_w^{i(b)}(\boldsymbol{\theta}) = w_{(b)}(\boldsymbol{\theta})\delta^{i(b)}(\boldsymbol{\theta}), \tag{11}$$

where $w_{(b)}(\boldsymbol{\theta})$ is the survey window function on the sky for bth tracer; $w_{(b)} = 1$ if the direction $\boldsymbol{\theta}$ on the sky is in the survey region, otherwise $w_{(b)} = 0$. With the two-dimensional Fourier components of $\delta_w^{i(b)}(\boldsymbol{\theta})$,

$$\tilde\delta_w^{i(b)}(\boldsymbol{\ell}) = \int {\rm d}^2\boldsymbol{\ell}\prime (2\pi)^{-2} \tilde w_{(b)}(\boldsymbol{\ell} - \boldsymbol{\ell}\prime)\tilde\delta^{i(b)}(\boldsymbol{\ell}\prime), \tag{12}$$

where $\tilde w_{(b)}$ and $\tilde\delta^{i(b)}$ are Fourier transform of $w_{(b)}$ and $\delta^{i(b)}$, respectively, we can define an estimator of the angular power spectrum as [18]

$$\hat C_{i(bb\prime)}(\boldsymbol{\ell}) = \frac{1}{\Omega_w^{(bb\prime)}} \int_{|\boldsymbol{\ell}\prime|\in\boldsymbol{\ell}} \frac{{\rm d}^2\boldsymbol{\ell}\prime}{\Omega_{\boldsymbol{\ell}}} \tilde\delta_w^{i(b)}(\boldsymbol{\ell}\prime)\tilde\delta_w^{i(b\prime)}(-\boldsymbol{\ell}\prime), \tag{13}$$

where we have considered the integral over a shell in the Fourier space of width $\Delta\boldsymbol{\ell}$ and volume

$$\Omega_{\boldsymbol{\ell}} = \int_{|\boldsymbol{\ell}\prime|\in\boldsymbol{\ell}} {\rm d}^2\boldsymbol{\ell}\prime \approx 2\pi\boldsymbol{\ell}\Delta\boldsymbol{\ell}. \tag{14}$$

Here the effective survey area was defined as

$$\Omega_w^{(bb\prime)} = \int {\rm d}^2\boldsymbol{\theta} w_{(b)} w_{(b\prime)}, \tag{15}$$

which is the survey area of the bth tracer for $b = b\prime$ and the overlapping area of the b and $b\prime$th tracers for $b \neq b\prime$. We have determined the functional form of the estimator so that it is unbiased in a sense that the ensemble average gives the true power spectrum, namely, $\langle \hat C_{i(bb\prime)}(\boldsymbol{\ell})\rangle = C_{i(bb\prime)}(\boldsymbol{\ell})$. Assuming the Gaussian error covariance, we obtain the covariance matrix for multiple tracers as

$$\begin{aligned}{\rm Cov}[C_{i(bb\prime)}(\boldsymbol{\ell}), C_{j(\tilde b\tilde b\prime)}(\boldsymbol{\ell}\prime)] &= \frac{\delta^{\rm K}_{ij}\delta^{\rm K}_{\boldsymbol{\ell}\boldsymbol{\ell}\prime}}{(2\boldsymbol{\ell}+1)\Delta\boldsymbol{\ell}} \frac{4\pi\Omega_w^{(bb\prime\tilde b\tilde b\prime)}}{\Omega_w^{(bb\prime)}\Omega_w^{(\tilde b\tilde b\prime)}} \\ &\times [C_{i(b\tilde b)}(\boldsymbol{\ell})C_{i(b\prime\tilde b\prime)}(\boldsymbol{\ell}) + C_{i(b\tilde b\prime)}(\boldsymbol{\ell})C_{i(b\prime\tilde b)}(\boldsymbol{\ell})],\end{aligned} \tag{16}$$

with

$$\Omega_w^{(bb\prime\tilde b\tilde b\prime)} = \int {\rm d}^2\boldsymbol{\theta} w_{(b)} w_{(b\prime)} w_{(\tilde b)} w_{(\tilde b\prime)}. \tag{17}$$

Since the observed spectrum includes the shot noise contamination, we replace $C_{i(bb\prime)}(\boldsymbol{\ell})$ with $C_{i(bb\prime)}(\boldsymbol{\ell}) + \bar N^{-1}_{i(b)}\delta^{\rm K}_{bb\prime}$.

IV. RESULTS

As we stated above, we consider the Euclid photometric survey and the SKA continuum survey. For Euclid, a redshift range $0.2 < z < z_{\rm max}$ is considered and galaxy samples are split into several redshift bins with the same interval ($\Delta z = 0.5$). We neglect the photometric redshift errors as they are expected to be much smaller than Δz. To include the effect of flux cut for each redshift range, we adopt the following minimum observed mass for each bin, $M_{\rm est} > 0.7, 1, 2, 5, 10, 20, 50, 100, \ldots$ in the unit of $10^{11}h^{-1}M_\odot$ and set $\Gamma^{\rm Euclid}_{(b)} = 1$. Galaxy samples are further split according the estimated halo mass. We consider five mass bins and take separating masses such that the five mass bins of the same redshift bin have the same number of samples. Here it should be noted that the separating masses depend on the redshift. We will discuss other possibilities of the mass binning later. Summation of the power spectrum is taken for an $\boldsymbol{\ell}$ range of $3 \le \boldsymbol{\ell} \le 400$.

As for the SKA continuum survey, we have only one redshift bin as no redshift information is available. Thus we simply drop the redshift dependent terms in Eqs. (4) and (5). Following [7], we consider five types of galaxies as five tracers with the typical masses [19], $M_{\rm SFG} = 10^{11}h^{-1}M_\odot$ for star forming galaxies, $M_{\rm RQQ} = 3\times10^{12}h^{-1}M_\odot$ for radio quiet quasars, $M_{\rm FRI} = 10^{13}h^{-1}M_\odot$ for FRI, $M_{\rm SB} = 5\times10^{13}h^{-1}M_\odot$ for starburst galaxies, and $M_{\rm FRII} = 10^{14}h^{-1}M_\odot$ for FRII. Accordingly, we consider five mass bins, $M_{(i)} < M < M_{(i+1)}$ $(i = 1, \ldots, 4)$ and $M > M_{(5)}$, with $M_{(1)} = 0.9\times10^{11}h^{-1}M_\odot$, $M_{(2)} = \sqrt{M_{\rm SFG}M_{\rm RQQ}}$, $M_{(3)} = \sqrt{M_{\rm RQQ}M_{\rm FRI}}$, $M_{(4)} = \sqrt{M_{\rm FRI}M_{\rm SB}}$, $M_{(5)} = \sqrt{M_{\rm SB}M_{\rm FRII}}$. For the flux cut, we adopt the gray body factor as $\Gamma^{\rm SKA1}_{(b)} = \{0.013, 0.03, 0.1, 1, 1\}$ and $\Gamma^{\rm SKA2}_{(b)} = \{0.5, 1, 1, 1, 1\}$, which are chosen to match the expected number density distribution of galaxies found in these surveys (see e.g., [7]). As for $\boldsymbol{\ell}$ range, we consider $2 \le \boldsymbol{\ell} \le 400$.

In computing the Fisher matrix for the combination of Euclid and SKA surveys, we adopt $9,000$ deg^2 as the area of the overlap region and we neglect the contributions from the derivative of the cross correlations between Euclid and SKA for simplicity. We focus on constraints on $f_{\rm NL}$ and marginalize over the other parameters.

Before showing expected constraints from Euclid and SKA surveys, let us check the dependence of the efficiency of the multitracer technique on the overlapping survey area and different mass binning, considering a simple case of two tracers observed by a Euclid-like survey. In Fig. 1, we plot the marginalized error on $f_{\rm NL}$ as a function of the overlap fraction $\Omega_w^{(12)}/\Omega_w$ for a single redshift bin $0.7 < z < 1.2$. Different curves represent different mass binning varying the mass ratio $M_{(2)}/M_{(1)}$. Here we assume that the sky coverages for both tracers are the same, $\Omega_w^{(11)} = \Omega_w^{(22)} \equiv \Omega_w$. We find that the nonvanishing overlap region leads to improved constraints on $f_{\rm NL}$, which becomes smallest in the case of the maximal overlap. One can also see that in the case of the maximal overlap there is a critical value of the mass ratio $M_{(2)}/M_{(1)}$ which results in the tightest constraint. This behavior can be understood as follows: once we fix the mass ratio, the number density for each mass bin, $\bar{N}_{i(b)}$, is determined through Eq. (6). Changing the value of the mass ratio leads to the larger shot noise for one of the mass bins and smaller shot noise for the other. We find that the tightest constraint is obtained when the shot noise for the two mass bins becomes comparative. This is the reason for our choice of separating masses by the same number density, as explained above.

Next, we focus on the Euclid survey. Figure 2 shows the marginalized constraints on $f_{\rm NL}$ as a function of the number of tracers for a single redshift bin $0.7 < z < 1.2$ with the maximal overlap among tracers. We find that the constraining power increases with N_M. Even 2 tracers drastically improve the constraint, simply because the multitracer technique does not take effect for the one tracer

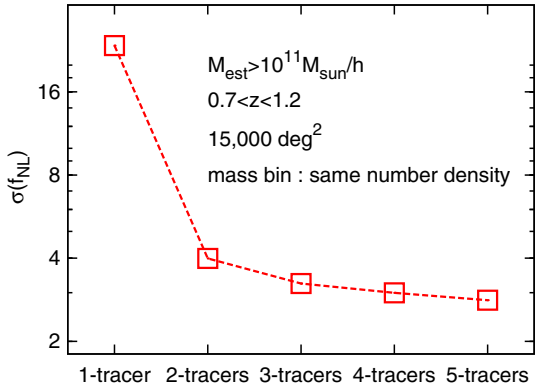

FIG. 2 (color online). The marginalized error on $f_{\rm NL}$ as the function of the number of the tracers in the single redshift bin $0.7 < z < 1.2$. The mass bins are divided such that they have the equal shot noises.

case. Furthermore, combining multiple redshift bins improves substantially the constraint, as is shown in Fig. 3. We find that galaxy samples as far as $z = 3.2$ (sixth bin) contribute significantly to the constraint. When five mass bins and eight redshift bins are taken into account, the Euclid photometric survey can reach $\sigma(f_{\rm NL}) = 0.46$. Although the use of galaxies out to $z = 4.2$ is probably too optimistic, even in a more realistic situation where we use redshift bins up to $z = 2.7$ (five bins) the improvement is still significant, $\sigma(f_{\rm NL}) = 0.66$. In the reminder of the paper we conservatively adopt $z_{\rm max} = 2.7$ as the maximal redshift for Euclid.

Finally, Fig. 4 shows the expected marginalized constraints on $f_{\rm NL}$ for each survey and their combinations. The constraints on $f_{\rm NL}$ from SKA1 and SKA2 are $\sigma(f_{\rm NL}) = 1.64$, 0.66, respectively, which are consistent with Ref. [7]. The results of SKA2 and SKA1 are comparable to or relatively weaker than that from Euclid, presumably because the redshift information obtained from the photometric survey is more advantageous than the larger sky coverage and the larger number of galaxy samples from

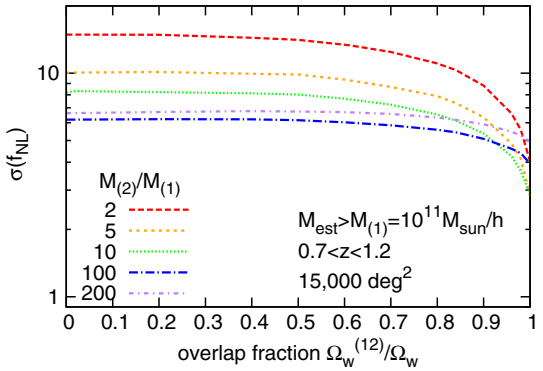

FIG. 1 (color online). The marginalized error on $f_{\rm NL}$ as the function of the overlap fraction, for the single redshift bin of $0.7 < z < 1.2$. Different lines show results with different mass ratio $M_{(2)}/M_{(1)}$.

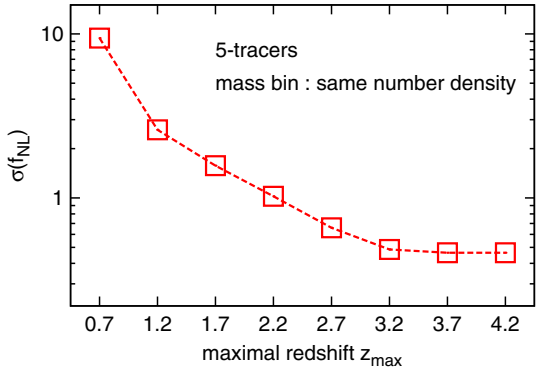

FIG. 3 (color online). The marginalized constraint on $f_{\rm NL}$ as a function of the maximum redshift, assuming the redshift range $0.2 < z < z_{\rm max}$ with width $\Delta z = 0.5$. Here we take five tracers (mass bins) for each redshift bin.

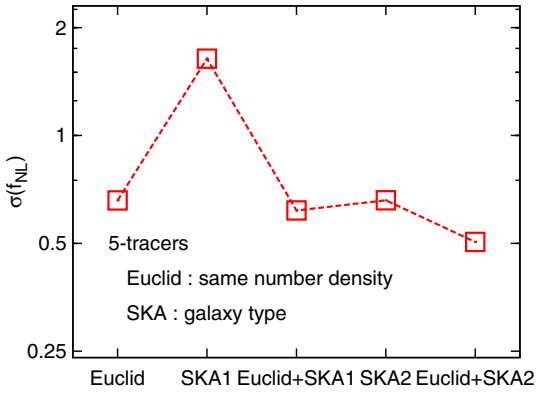

FIG. 4 (color online). The expected marginalized constraints on $f_{\rm NL}$ for each survey and combinations.

SKA survey. Combining Euclid and SKA, the constraint can improve further to $\sigma(f_{\rm NL}) = 0.61$ (Euclid + SKA1), 0.50 (Euclid + SKA2), suggesting that the joint analysis between Euclid and surveys are quite effective to constrain primordial non-Gaussianity. We again note that the improvement of the constraint is mainly due to the availability of the multiple tracer, as seen in Fig. 2. Although the results presented would be sensitive to the assumptions we considered in this paper, the constraining power due to the multitracer technique is expected to be generic and the behavior of the results would remain the same.

V. SUMMARY

To summarize, we have discussed the potential power of the multitracer technique for the combination of the Euclid photometric survey and the SKA continuum survey. Splitting the galaxy samples into the subsamples by the inferred halo mass and redshift, constraints on $f_{\rm NL}$ drastically improve. We have shown that constraints of $\sigma(f_{\rm NL}) = \mathcal{O}(1)$ can be obtained even with a single survey. Combining Euclid and SKA, even stronger constraints of $\sigma(f_{\rm NL}) = \mathcal{O}(0.1)$ can be obtained.

In this paper, we have made several simplified assumptions. In future galaxy surveys, the systematic uncertainties likely play a more important role than statistical errors. Here we considered only the uncertainty in the halo mass estimation. For instance, the uncertainty in photometric redshifts and the effect of the stochastic bias may become important. We should also address the identification of the optical and infrared counterparts in the overlap region of SKA and Euclid surveys. While we conservatively assumed no redshift information for the SKA survey, checking the counterparts in Euclid or other surveys would provide valuable information on redshifts of individual SKA sources, which may allow the tomographic analysis in the SKA survey to lead further improvements of the constraints (see [20]). We hope to come back to these issues in the near future.

ACKNOWLEDGMENTS

D. Y. is supported by Grant-in-Aid for Japan Society for the Promotion of Science Fellows (No. 259800). This work was supported by Grant-in-Aid from the Ministry of Education, Culture, Sports, Science and Technology (MEXT) of Japan, No. 24340048 (K. T.), No. 26610048 (K. T.), and No. 26800093 (M. O.).

[1] P. A. R. Ade *et al.* (Planck Collaboration), arXiv:1303.5084.
[2] N. Dalal, O. Dore, D. Huterer, and A. Shirokov, Phys. Rev. D **77**, 123514 (2008).
[3] V. Desjacques, U. Seljak, and I. Iliev, Mon. Not. R. Astron. Soc. **396**, 85 (2009).
[4] S. Ho, N. Agarwal, A. D. Myers, R. Lyons, A. Disbrow, H.-J. Seo, A. Ross, C. Hirata *et al.*, arXiv:1311.2597.
[5] T. Giannantonio, A. J. Ross, W. J. Percival, R. Crittenden, D. Bacher, M. Kilbinger, R. Nichol, and J. Weller, Phys. Rev. D **89**, 023511 (2014).
[6] U. Seljak, Phys. Rev. Lett. **102**, 021302 (2009).
[7] L. D. Ferramacho, M. G. Santos, M. J. Jarvis, and S. Camera, arXiv:1402.2290.
[8] D. J. Eisenstein and W. Hu, Astrophys. J. **496**, 605 (1998).
[9] R. K. Sheth and G. Tormen, Mon. Not. R. Astron. Soc. **308**, 119 (1999).
[10] M. LoVerde, A. Miller, S. Shandera, and L. Verde, J. Cosmol. Astropart. Phys. 04 (2008) 014.
[11] M. Oguri, Phys. Rev. Lett. **102**, 211301 (2009).
[12] S. Chongchitnan and J. Silk, Astrophys. J. **724**, 285 (2010).
[13] A. Vale and J. P. Ostriker, Mon. Not. R. Astron. Soc. **353**, 189 (2004).
[14] A. Leauthaud, J. Tinker, K. Bundy *et al.*, Astrophys. J. **744**, 159 (2012).
[15] M. Lima and W. Hu, Phys. Rev. D **70**, 043504 (2004).
[16] M. Oguri and M. Takada, Phys. Rev. D **83**, 023008 (2011).
[17] C. Cunha, D. Huterer, and O. Dore, Phys. Rev. D **82**, 023004 (2010).
[18] M. Takada and W. Hu, Phys. Rev. D **87**, 123504 (2013).
[19] R. J. Wilman, L. Miller, M. J. Jarvis, T. Mauch, F. Levrier, F. B. Abdalla, S. Rawlings, H. -R. Kloeckner, D. Obreschkow, D. Olteanu, and S. Young, Mon. Not. R. Astron. Soc. **388**, 1335 (2008).
[20] A. Raccanelli, O. Dore, D. J. Bacon, R. Maartens, M. G. Santos, S. Camera, T. Davis, M. J. Drinkwater *et al.*, arXiv:1406.0010.